

Coherent backscattering of light by resonant atomic dipole transitions

David Wilkowski, Yannick Bidel,* and Thierry Chanelière

Laboratoire Ondes et Désordre, FRE 2302 Centre Nationale de la Recherche Scientifique, 1361 Route des Lucioles, F-06560 Valbonne, France

Dominique Delande and Thibaut Jonckheere**

Laboratoire Kastler Brossel, Tour 12, Etage 1, Université Pierre et Marie Curie, 4 Place Jussieu, F-75005 Paris, France

Bruce Klappauf,* Guillaume Labeyrie, and Christian Miniatura**

Laboratoire Ondes et Désordre, FRE 2302 Centre Nationale de la Recherche Scientifique, 1361 Route des Lucioles, F-06560 Valbonne, France

Cord Axel Müller

Physikalisches Institut, Universität Bayreuth, D-95440 Bayreuth, Germany

Olivier Sigwarth

Laboratoire Kastler Brossel, Tour 12, Etage 1, Université Pierre et Marie Curie, 4 Place Jussieu, F-75005 Paris, France

Robin Kaiser

Laboratoire Ondes et Désordre, FRE 2302 Centre Nationale de la Recherche Scientifique, 1361 Route des Lucioles, F-06560 Valbonne, France

Received May 5, 2003; revised manuscript received July 24, 2003; accepted July 25, 2003

We study coherent backscattering (CBS) of resonant light by cold atomic vapors, both experimentally and theoretically. The theory predicts a drastic reduction of the CBS enhancement factor when a degenerate internal structure is present in the ground state. We test this prediction in experiments using different atoms and various transitions. © 2004 Optical Society of America

OCIS codes: 140.3320, 030.1670, 030.6600.

1. INTRODUCTION

The study of quantum transport is a very active field of research including, beyond mesoscopic¹ and nanoscopic physics, the study of photonic crystals^{2,3} as well as the propagation of waves in random media.⁴ One particular aspect is localization, i.e., the inhibition of coherent transport as the result of interferences. This effect can be achieved either with well-structured systems, which has led to the field of photonic crystals, or with random systems in which a disorder-induced phase transition connects conducting systems to insulating systems. In both cases the degree of dimension of the system has a strong influence on the localization criterion. In one-dimensional systems localization in well-structured media corresponds to the well-known Bragg reflection. For one-dimensional random systems, localization is also expected to occur even for very small disorder. In these one-dimensional systems, the system size needs to be larger than a characteristic length, depending on reflection

coefficients and disorder. The three-dimensional case is very different, as now one expects a critical reflection coefficient for well-structured systems and a critical disorder for random systems for the localization to occur. This made the experimental and theoretical investigation of three-dimensional systems more challenging, and many questions are still not clearly answered. The underlying physics is very similar for various waves: acoustic, electronic, electromagnetic, seismic, and neutral-atom matter waves.⁵ However, differences appear when one takes into account the precise dispersion relation and the tensor nature of the wave and the interaction in the case of electrons. Electromagnetic waves present several advantages for the study of the fundamental properties of localization that made this field of research very attractive in recent years. With respect to experimental and theoretical progress, the well-structured systems have been understood to a large extent, and experimental devices can now be produced in the visible domain. For dis-

ordered systems, however, only one observation⁶ of the disorder-induced transition in three dimensions has been reported, with further investigation required because of possible residual absorption.^{7,8}

As disordered atomic systems are free from many defects inherent to solid state samples, we have therefore chosen to study wave transport of light in such systems. The first experimental observation of coherent backscattering (CBS), which shares common features with weak localization, was reported in 1999.⁹ This opened the way for more experiments to follow.^{10–14} The quantum nature of the system has been identified as the origin of a new kind of reduction of the enhancement factor for CBS.¹⁵ Qualitative analysis^{16–18} and quantitative¹⁹ comparison with experiments have successfully been performed. In this paper we report on the experimental measurement of the CBS enhancement factor for various atomic transitions. We also give the theoretical prediction for any single atomic transition and compare results of Monte Carlo (MC) simulations with our experimental data. The experimental and numerical results shown in this paper thus represent our complete set of data available to date on CBS of light by cold atoms, illustrating in detail the influence of the internal structure of the atoms.

This paper is organized as follows. In Section 2 we recall the basic principles for the calculation of the CBS signal, including the description of the particular aspect when atomic scatterers are involved. In Section 3 we describe the principle of our MC simulation, a necessary technique when one attempts a quantitative comparison between theory and experiment. Section 4 is devoted to the description of the experiments. The comparison of the CBS data obtained with laser-cooled rubidium and strontium vapors and different transitions confirms the validity of the theoretical treatment.

2. COHERENT BACKSCATTERING AND ATOMIC DIPOLE TRANSITIONS

When a wave is scattered from a disordered medium, the interference between all partial waves creates its “fingerprint,” the speckle pattern. An average over random configurations washes out the interferences between waves that have traveled along different scattering paths, which produces the smooth, diffuse intensity that is familiar to us from the view of natural objects such as clouds or white paint—with one exception: In exactly the backscattering direction, partial waves that have traveled along the same scattering paths but in opposite directions have no phase difference. The two waves interfere constructively for *all* paths so that this coherent backscattering (CBS), as it is termed, survives the configuration averaging and can be observed in an angular range $\Delta\theta \approx 1/kl$ around the backscattering direction (k is the wave vector, l the mean free path inside the medium). Under optimal experimental conditions, the CBS enhancement factor—defined as the ratio of total intensity at backscattering and the background far from backscattering—is 2.

To calculate the average backscattered intensity, it is in principle possible to write down the scattered speckle intensity for a fixed random configuration and average afterwards over a sufficiently large ensemble. But since

CBS is a phenomenon that generally involves high orders of multiple scattering, this naive procedure is analytically intractable and numerically too costly. A much more efficient method is to calculate directly the moments of the multiply scattered field G , i.e., the average amplitude $\langle G \rangle$, the average intensity $\langle G^*G \rangle$, etc., in a way that may be sketched as follows²⁰:

1. The average amplitude $\langle G \rangle$ evolves inside an effective medium characterized by a complex refractive index. In a sufficiently dilute medium (such that $1/kl \ll 1$), the refractive index can be calculated from the average microscopic scattering T -matrix of a single scatterer since repeated scattering from the same object may be neglected. The imaginary part of the refractive index (proportional to the inverse of the scattering mean-free-path l) describes the scattering out of the average propagating mode $\langle G \rangle$ with total scattering cross section σ_{tot} .

2. If we neglect interference in a first step, we can say the average intensity $\langle G^*G \rangle$ propagates with the modulus squared $|\langle G \rangle|^2$ of the average amplitude calculated in step 1 between scattering processes. There, the average intensity $\langle G^*G \rangle$ changes its direction of propagation according to the average differential cross section $\langle d\sigma/d\Omega \rangle$ of a single scatterer.

3. The CBS contribution of counterpropagating amplitudes is obtained from the result of step 2 by a time-reversal operation on one of the two amplitudes that may require some careful bookkeeping of wave vectors, polarization vectors, internal degrees of freedom, etc. Under optimal conditions (exact backscattering, parallel polarization, no internal degeneracy) the CBS contribution of any scattering order is equal to its counterpart in step 2. Then, a large CBS enhancement can be observed (up to two).

This procedure permits us to obtain analytical expressions for the intensity scattered whenever the medium has a sufficiently simple geometry—in practice, one is limited to the simple cases of an infinite half-space or a slab of finite depth.²¹ A very important characteristic of the above procedure is its self-consistency: The refractive index used in step 1 and the average cross section used in step 2 are linked by an energy conservation relation that generalizes the optical theorem, valid for the scattering by an isolated, bounded object, to the above case of an effective medium. In the absence of absorption, the procedure simply states that every photon that has disappeared from the propagating beam has been scattered in another direction, and it takes the familiar form $l = 1/n\sigma_{\text{tot}}$, where n is the number density of scatterers with total elastic scattering cross section σ_{tot} .

The first experiments of CBS with cold atoms have already shown that the microscopic properties of the atoms strongly influence the coherent light transport. Atoms have dipole transitions with extremely sharp resonances, which are welcome since they permit strong scattering with cross sections of the order of $\sigma_{\text{tot}} \sim \lambda^2$. But the ground and excited levels usually have a large Zeeman degeneracy, resulting in a more complex situation since all possible transitions between sublevels and their coupling to the light polarization have to be considered. The configuration average over all realizations of the scatter-

ing medium then must include the internal atomic quantum numbers. For arbitrary distributions, a numerical calculation of the internal configuration average would have to be performed. But inside an optically thick atomic cloud, the atoms are expected to be distributed statistically, i.e., with equal probability over their internal states. In this case, the internal average restores the local invariance under rotations and can be done analytically. Indeed, the average differential cross section for the scattering of a photon with polarization ϵ to ϵ' from an arbitrary closed dipole transition $F \rightarrow F'$ reads¹⁶

$$\left\langle \frac{d\sigma}{d\Omega} \right\rangle = \frac{3\sigma_{\text{tot}}}{8\pi} (w_1 |\epsilon' \cdot \epsilon^*|^2 + w_2 |\epsilon' \cdot \epsilon|^2 + w_3), \quad (1)$$

where the information about the internal degeneracy is contained in the coefficients $w_i(F, F')$. For transitions of the type $F \rightarrow F' = F + 1$, they are

$$w_i = \frac{1}{10(F+1)(2F+1)} \begin{cases} (6F^2 + 17F + 10) & i = 1 \\ [-4F(F+2)] & i = 2 \\ [F(6F+7)] & i = 3 \end{cases} \quad (2)$$

An $F = 0 \rightarrow F' = 1$ dipole transition corresponds to $w_1 = 1$, $w_{2,3} = 0$, and we recover the well-known case of an isotropic dipole scatterer. The self-consistency or energy conservation mentioned above here implies the sum rule $w_1 + w_2 + 3w_3 = 1$. The CBS contribution (see step 3 of the above procedure) involves the same average scattering cross section but with exchanged coefficients $w_2 \leftrightarrow w_3$. It is evident that $w_2 \neq w_3$ for any finite $F > 0$, such that the CBS contrast will be reduced. Figure 1 shows the CBS enhancement factor for the four usual polarization channels and closed dipole transitions of the type $F' = F + 1$ in the simple geometry of an infinite half-space. The four polarization channels are defined by the incident and detected polarization of the light: two linear channels with a linear incident polarization and the detected polarization either parallel ($lin \parallel lin$) or orthogonal ($lin \perp lin$) to the incident polarization, and two circular channels where the helicity of the detected light is either the same ($h \parallel h$) or opposite ($h \perp h$) to the incident

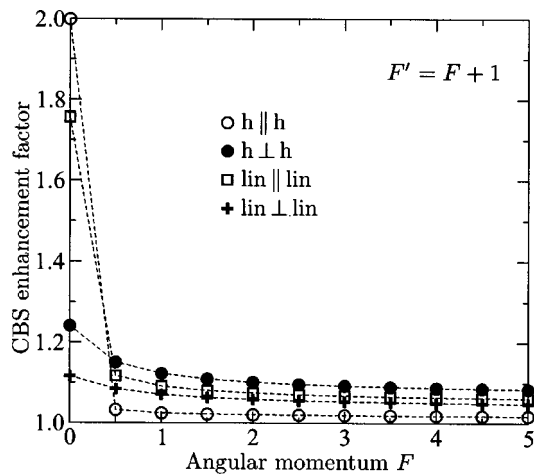


Fig. 1. Theoretical CBS enhancement for various transitions and polarization channels. These results are obtained analytically for a semi-infinite medium (all scattering orders included).

helicity. The reduction with respect to the nondegenerate isotropic dipole $F = 0$ is dramatic.

However, in the case of light scattering by cold atoms, the atomic cloud does not have the simple slab geometry, but rather a spherical symmetry. Moreover, the cloud has an inhomogeneous average density that decreases from its maximum value at the trap center towards zero roughly like a Gaussian. This unusual geometry influences the CBS peak height and shape, and must be taken into account for a quantitative comparison between theory and experiment, as explained in Section 3.

3. MONTE CARLO SIMULATION

Although the fundamental processes at work in the atom–light interaction are well understood, an exact calculation of the CBS cone is in general impossible. This is because the scattering medium—in our case a cold atomic gas produced in a magneto-optical trap (MOT)—has a rather complicated shape. The density of scatterers is maximal at the center of the trap and has approximately an isotropic Gaussian distribution

$$n(\mathbf{r}) = n_0 \exp\left(-\frac{\mathbf{r}^2}{2r_0^2}\right), \quad (3)$$

where n_0 is the density at the center of the trap and r_0 the rms radius of the trap. The maximum optical thickness of the sample is obtained along a diameter:

$$b = \sqrt{2\pi} n_0 \sigma_{\text{tot}} r_0. \quad (4)$$

We chose to use a MC method to calculate the enhancement factors, shapes, and angular widths of various CBS cones. On the other hand, our numerical calculation takes into account exactly the internal structure of the atom. Since all possible hyperfine dipole transitions are well separated on the scale of the linewidth Γ , we consider only quasi-resonant light scattering induced by a closed hyperfine transition. When an atom scatters the incoming light, the atom may stay in the same Zeeman sublevel—this is a Rayleigh transition—or change its magnetic quantum number—this is a degenerate Raman transition. In both cases, at weak laser intensities, and if recoil and Doppler effects are negligible (which one expects to be the case for our cold atomic cloud), the scattered photon has the same frequency as the incoming photon: the scattering is elastic. The scattering amplitude by a single atom depends on the initial and final Zeeman sublevels, on the scattering direction, and on the incident and scattered polarizations.¹⁶ As the atoms produced in a MOT are not in well-defined internal states, but rather in a statistical mixture of Zeeman states, the calculation of the CBS cone requires, in addition to the usual position averaging, an averaging over the possible internal ground states of the atom. We perform the average over the positions of the scatterers with a MC method and the average over the internal degree of freedom analytically by employing the average atomic scattering vertex.^{16,17} The details of the method are given in Ref. 13. The essential assumption is that all Zeeman sublevels in the ground state are equally populated, without any coherence between sublevels. This is a reasonable assumption pro-

vided no optical pumping takes place in the medium. Our MC method is flexible, as it makes it possible to compute the CBS cone for an arbitrary spatial repartition of the scatterers. It is important to note that all the parameters in the numerical calculations (optical thickness of the medium, shape and dimensions of the atomic cloud, and geometrical properties of the incoming laser beam) have been experimentally measured, which means that the CBS cones that we calculate have no adjustable parameter.

The algorithm basically consists of launching a photon randomly on the atomic gas (with a probability distribution given by the incoming laser beam), letting it propagate in the medium according to the Green's function discussed above, selecting randomly the position of the first scattering event, scattering it in a random direction and with a random polarization chosen according to the probability law in Eq. (1), letting it propagate until it reaches the (randomly chosen) next scatterer, etc. The full procedure is restarted as soon as the photon exits the medium. Because the mean free path is not constant inside the medium, the propagation in the medium is not a simple exponential decay, but rather the cumulative extinction following the path of the photon, which is trivially calculated once the density of scatterers is known.

Along each multiply scattered path, the contribution to the experimental signal is computed. For the background (outside the CBS cone), it is simply the intensity of light carried by the path (the so-called ladder diagrams or step 2 of the calculation procedure discussed above), which means that interference effects are not present. On the other hand, we also calculate the contributions of the so-called maximally crossed diagrams (step 3), which are the dominant contributions to the CBS cone: They arise from the interference between a path and its time-reversed companion. In the MC calculation, we thus compute along each path not only the (squared) amplitude of the direct path, but simultaneously the interference term between the direct and the reverse amplitudes. Special care is needed when considering the polarization state of the photons. Indeed, given a multiple scattering path, the contributions of the possible polarizations of the photon must be carefully taken into account. This implies that two polarization tensors (one for the ladder contribution and one for the crossed contribution) must be simultaneously propagated in the MC calculation. The ladder polarization tensor is characterized by the three coefficients $w_{1,2,3}$ described above. The crossed polarization tensor is easily handled in the MC calculation through the substitution $w_2 \leftrightarrow w_3$.¹⁶ Altogether, the extra cost to be paid for atomic scatterers is rather modest. Note that, even for parallel polarization channels, the complication introduced by the atomic structure breaks the equality of the ladder and crossed contributions at exact backscattering. This is why enhancement factors smaller than 2 (and usually much smaller than 2, except for the $F = 0 \rightarrow F' = 1$ transition) are observed.

We have checked the consistency of our approach by performing the average over the internal degrees of freedom by a MC approach instead of using the analytically known scattering vertex. In this alternative approach, the internal Zeeman substate of each scatterer is chosen

randomly (with a uniform distribution), and the photon is scattered randomly following the scattering cross section of this specific Zeeman substate. We checked in simple cases that this naïve approach gives exactly the same results as the more sophisticated method using the analytically known scattering vertex. Of course, the sophisticated method is much more efficient and a CBS cone can be calculated in a few minutes of computer time with an excellent signal-to-noise ratio. On the other hand, the naïve method is more flexible. For example, it makes it possible to compute separately the contributions involving only Rayleigh transitions and the contributions in which at least one atom makes a degenerate Raman transition and ends in a different Zeeman substate.

4. EXPERIMENTS

A. Experimental Procedure

The experimental setups and procedures used to record CBS signals are essentially the same in the rubidium and strontium experiments, and have been described elsewhere.^{9,11} We illuminate the atomic cloud with a quasi-resonant, collimated, Gaussian beam whose polarization is usually linear or circular. The backscattered light is collected through a beam splitter and directed onto a cooled CCD. The far-field intensity distribution is readily obtained by placing the CCD in the focal plane of a lens. The detected light polarization state can be selected: It is usually either parallel or orthogonal to the incident state. The experiment time sequence includes a preparation period (10–30 ms) in which the atoms are trapped and cooled and a detection period (≈ 1 ms) in which the MOT is switched off and the CBS cone recorded. This detection window is short enough that most of the atoms are recaptured when the MOT is switched back on. The CBS image is obtained with one single CCD exposure covering several thousand of such preparation–detection cycles. A synchronized mechanical chopper blocks the CBS detection path while the trap is on to shield the detector from the intense fluorescence from the MOT. To remove stray light contributions, we subtract from the CBS image a background image taken in identical conditions but without cold atoms. To improve the signal statistics and extract reliable measurements of the cone contrast and angular width, we can perform an angular average of the image. This procedure is valid as long as the CBS peak is azimuthally symmetric around its center. As will be seen later (Subsection 4.C), this is not always the case.

The rubidium MOT ($\lambda = 780$ nm) is loaded from a dilute thermal vapor in a quartz cell. By using six large laser beams (diameter 4 cm, total power 200 mW), we are able to trap up to 7×10^9 Rb⁸⁵ atoms in a quasi-Gaussian cloud of FWHM 5–7 mm and rms velocity $v_{\text{rms}} \approx 0.15$ m/s. The optical thickness, which determines the amount of multiple scattering inside the sample, is routinely 30–40 on the $F = 3 \rightarrow F' = 4$ transition of the D₂ line. It is quite straightforward to trap either of isotopes Rb⁸⁵ and Rb⁸⁷. Using these two isotopes on the D₂ line, one has several transitions which can be explored. One can start from the ground state Rb⁸⁵ ($F = 2$), Rb⁸⁵ ($F = 3$), Rb⁸⁷ ($F = 1$), or Rb⁸⁷ ($F = 2$) and couple to

all excited states with $F' = F - 1, F, F + 1$. However, as we typically need to scatter 100 photons per atom to accumulate the input for our CBS signal, we are restricted to the use of closed transitions, leaving in principle four different transitions. In practice one of these four ($F = 1 \rightarrow F' = 0$) is too close in detuning to an open transition, leaving three transitions that have been explored: $\text{Rb}^{85} (F = 3 \rightarrow F' = 4)$, $\text{Rb}^{85} (F = 2 \rightarrow F' = 1)$, and $\text{Rb}^{87} (F = 2 \rightarrow F' = 3)$.

The strontium MOT ($\lambda = 461 \text{ nm}$) is loaded from a thermal beam produced by an oven ($T = 500^\circ \text{C}$), which is then slowed down to a few m/s using Zeeman cooling. Three different isotopes have been trapped: Sr^{86} , Sr^{87} , and Sr^{88} . The atomic sample of Sr^{88} contains $10^7 - 10^8$ atoms for a FWHM of 1 mm and a rms velocity of $v_{\text{rms}} \approx 1.7 \text{ m/s}$, much larger than in the rubidium experiment because of the lack of sub-Doppler Sisyphus cooling effects relying on the degeneracy of the ground state of the atoms. The maximal optical thickness with Sr^{88} is currently ≈ 3 . In the case of strontium, the ground state has zero electronic spin ($S = 0$) and we excite a $L = 0 \rightarrow L' = 1$ transition. For the bosonic isotopes (Sr^{86} , Sr^{88}) with zero nuclear spin ($I = 0$), this corresponds to a $F = 0 \rightarrow F' = 1$ transition, whereas for the fermionic isotope (Sr^{87}) with $I = 9/2$, the $F = 9/2 \rightarrow F' = 7/2$, $F' = 9/2$, and $F' = 11/2$ transitions are excited. As the optical thickness for the fermionic isotope Sr^{87} is well below unity in the present setup, we have not been able, up to now, to exploit this isotope for coherent backscattering. The Sr^{86} and Sr^{88} isotopes both have a $F = 0 \rightarrow F' = 1$ transition and are thus equivalent with respect to coherent backscattering.

B. Coherent Backscattering Enhancement and Width

Figure 2 shows the CBS profiles (circles, angular average) obtained from a sample of Rb^{85} (optical thickness = 26)

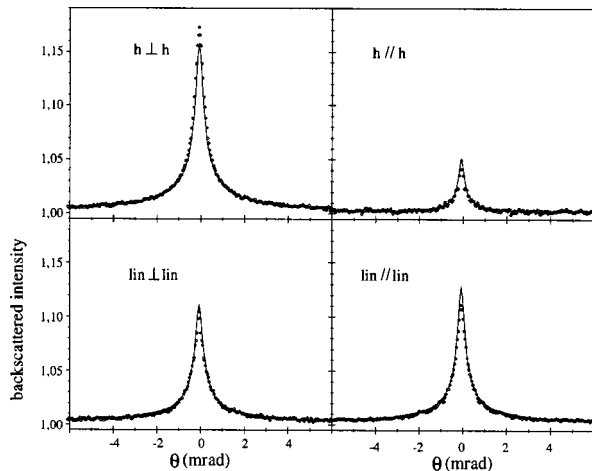


Fig. 2. CBS profiles for Rb^{85} , $F = 3 \rightarrow F' = 4$. We show the CBS profiles (circles, angular averages) in the four standard polarization channels obtained by exciting the $F = 3 \rightarrow F' = 4$ transition of the D_2 line of Rb^{85} (cloud optical thickness $b = 26$). The small enhancement factors observed in all channels is a direct consequence of the atomic internal structure. MC simulations (solid curves) including the parameters of the experiment (no adjustable parameters) show excellent overall agreement.

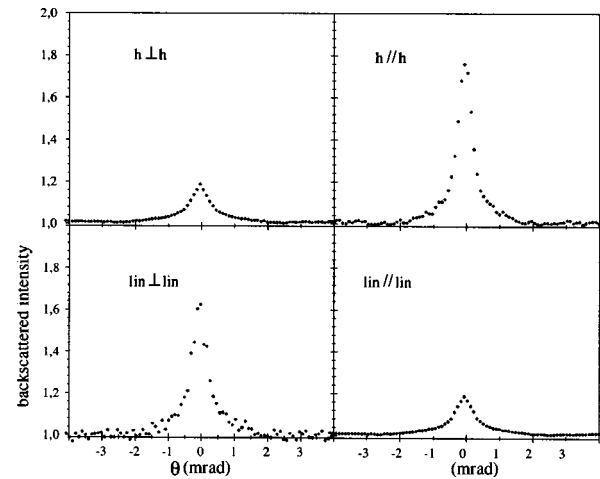


Fig. 3. CBS profiles for Sr^{88} , $F = 0 \rightarrow F' = 1$. We plot here the CBS profiles (circles, angular averages) in the four polarization channels obtained with the $F = 0 \rightarrow F' = 1$ transition of Sr^{88} (cloud optical thickness $b = 3$). In the absence of an internal structure in the ground state, an enhancement factor close to 2 is recovered in the $h \parallel h$ channel, as is the case with classical samples.

for light tuned to the $F = 3 \rightarrow F' = 4$ transition of the D_2 line. Note the small enhancement factor in all channels, especially in the $h \parallel h$ channel where it is only 1.05 instead of the 2 for classical samples. These small values result from two processes: (1) the contrast reduction mechanism described in Section 2, which is a fundamental consequence of atomic level degeneracy, and (2) the single-scattering contribution that is present in all channels as a result of the degenerate Raman transition. Indeed, as shown by Eq. (1), there is no zero in the differential cross section for backward scattering as soon as $w_{2,3} \neq 0$, i.e., for any transition other than $F = 0 \rightarrow F' = 1$. The solid curves are the MC simulations with the parameters of the cloud, i.e., without any adjustable parameter, as noted above.

In Fig. 3 we plot the results of a CBS experiment on a cold cloud of Sr^{88} for which we used light resonant with the $F = 0 \rightarrow F' = 1$ transition. As can be immediately seen, in the absence of an internal structure in the ground state, one recovers an enhancement factor close to the theoretical value of 2 in the $h \parallel h$ channel. This finding is an important confirmation of the validity of the theory developed above.

We have also performed CBS experiments on other atomic systems. For instance, Fig. 4 shows the CBS profiles obtained with Rb^{87} ($F = 2 \rightarrow F' = 3$), together with the MC simulations. The overall result is very similar to the data of Fig. 2, as expected from the theory (see Fig. 1). One can note that the relative values of the enhancement factor between the four polarization channels are in excellent agreement with the MC simulation. However, a small overall difference appears: The experimental values are slightly above those of the MC simulation in Fig. 4. Several systematic effects can be invoked to explain such a difference, e.g., a nonuniform distribution among the Zeeman sublevels or optical pumping induced by the CBS probe. A more detailed analysis of different possible effects not included in the present MC simulation is presented in Ref. 13.

We have also verified that the $F = 0 \rightarrow F' = 1$ transition for the Sr^{86} isotope exhibits the expected enhancement factor of 2 in the helicity-preserving channel as predicted for any closed $F = 0 \rightarrow F' = 1$ transition.

In Table 1 we summarize the results of all our measurements and compare them to the analytical prediction for a semi-infinite medium including all scattering orders. As the finite size and the geometry of our samples have a measurable effect on the enhancement factor, we also show the results of MC simulations (based on the theory described in Section 2). The parameters included in the MC simulation are different for each experiment, taking into account the respective values of optical thickness and sample size. The results for the $F = 0 \rightarrow F' = 1$ transition are published in Ref. 11, those for the $F = 3 \rightarrow F' = 4$ transition in Ref. 19. The new simulations for the $F = 2 \rightarrow F' = 3$ and $F = 2 \rightarrow F' = 1$ transitions use an optical thickness of $b = 26$ and the same geometry as for the $F = 3 \rightarrow F' = 4$ transition. The MC approach is necessary to take into account the distribution of scattering orders in the sample and their relative contribution to the CBS interference. In the absence of internal structure and in the $h\parallel h$ channel, all orders have the same, maximal contribution to the interference, and the enhancement factor is independent of the optical thickness. This explains the good agreement between the theoretical prediction for a semi-infinite medium and the experimental data for the $F = 0 \rightarrow F' = 1$ transition in this polarization channel, even though the optical thickness in the experiment is only $b = 3$. This also is at the origin of the large discrepancy in particular in the two linear channels, as the various orders of scattering contributing to the cone differ a lot between a semi-infinite medium and a cloud of optical thickness of $b = 3$. On the other hand, in the $F > 0$ case (and in all polarization channels), the contribution to the interference decreases exponentially with increasing scattering order.¹³ Thus, the CBS peak for an optically thick sample is still dominated by double scattering, and one finds that the CBS enhancement is roughly constant for $b > 10$, with a slow decrease for larger b towards the limit corresponding to the semi-infinite medium (see Fig. 1).¹⁹

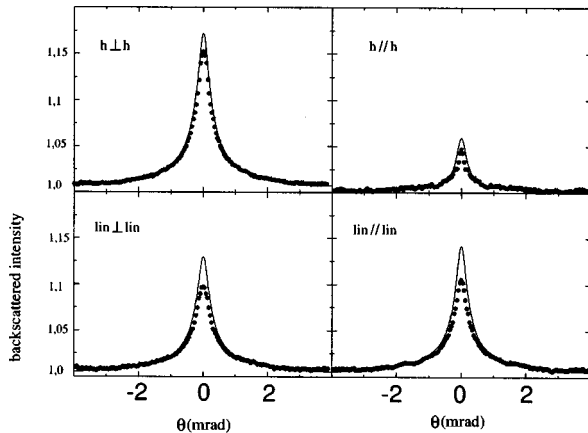


Fig. 4. CBS profiles for Rb^{87} , $F = 2 \rightarrow F' = 3$. The observed CBS peaks are very similar to those of Fig. 2 in all polarization channels. The MC simulations (solid curves) show good overall agreement.

Table 1. Coherent Backscattering Enhancement Factor

Transition	Channel	Enhancement Factor		
		Theory ^a	MC	Experiment
0-1'	$h\parallel h$	2.00	1.87	1.77
0-1'	$h\perp h$	1.24	1.19	1.17
0-1'	$lin\parallel lin$	1.76	1.22	1.17
0-1'	$lin\perp lin$	1.12	1.62	1.59
2-3'	$h\parallel h$	1.03	1.06	1.05
2-3'	$h\perp h$	1.10	1.17	1.15
2-3'	$lin\parallel lin$	1.08	1.14	1.10
2-3'	$lin\perp lin$	1.06	1.13	1.09
3-4'	$h\parallel h$	1.02	1.05	1.05
3-4'	$h\perp h$	1.09	1.16	1.17
3-4'	$lin\parallel lin$	1.07	1.13	1.11
3-4'	$lin\perp lin$	1.05	1.11	1.10
2-1'	$h\parallel h$	1.01	1.02	1.01
2-1'	$h\perp h$	1.04	1.07	1.05
2-1'	$lin\parallel lin$	1.03	1.06	1.03
2-1'	$lin\perp lin$	1.02	1.04	1.02

^aCBS enhancement factors obtained from the analytical theory for a half-space (Theory), the Monte Carlo simulation for the finite atomic cloud (MC), and the experiment (Experiment). All transitions are of the $F \rightarrow F' = F + 1$ type, except for the data corresponding to the $F = 2 \rightarrow F' = 1$ of Rb^{85} . Results for $F = 0 \rightarrow F' = 1$ correspond to Sr^{88} , those for $F = 2 \rightarrow F' = 3$ to Rb^{87} , and those for $F = 3 \rightarrow F' = 4$ and $F = 2 \rightarrow F' = 3$ to Rb^{85} .

Let us now address the question of the respective contribution of Rayleigh transitions (no change of internal state) and degenerate Raman transitions (change of internal state) in the CBS interference. Indeed, CBS is a two-wave interference phenomenon involving several atoms and a photon multiply scattered by these atoms along two time-reversed paths. The two paths interfere if and only if the final states along the two paths are not orthogonal. This implies in particular that the atomic states after the multiple scattering must be identical along the two reversed scattering paths. This implies in turn that each atom makes the same type of transition along the two paths. On the other hand, there is no necessity that the final atomic state be identical to the initial atomic state. Thus, an atom may well perform a degenerate Raman transition (the same one along the two reversed paths) and contribute to the CBS signal. The theory summarized in Section 2 treats both Rayleigh and Raman contributions on the same footing and predicts a Raman component of the CBS peak that can even dominate, depending on the polarization channel.¹⁶ Whereas it is difficult to isolate analytically the consequences of including Raman processes, this can easily be done in a MC simulation. Figure 5 shows MC simulations of the CBS peaks in the $h\parallel h$ channel for a spherical sample of uniform density and optical thickness $b = 10$ ($F = 3 \rightarrow F' = 4$ of Rb^{85}). The bold curve corresponds to both Rayleigh and Raman processes, while the light curve is ob-

tained by removing the Raman contribution to the interference (i.e., the incoherent Raman approach). The peak without Raman contribution is clearly not consistent with the observed signal (see Fig. 2).

C. Cone Symmetries

So far, we have analyzed the height and width of the CBS peak but not its azimuthal shape. The CBS signal is proportional to the Fourier transform of the diffuse intensity distribution on the front surface of the sample. Since low orders of scattering have an important contribution in CBS, this intensity distribution is affected by possible anisotropies in the radiation pattern, as in the case for di-

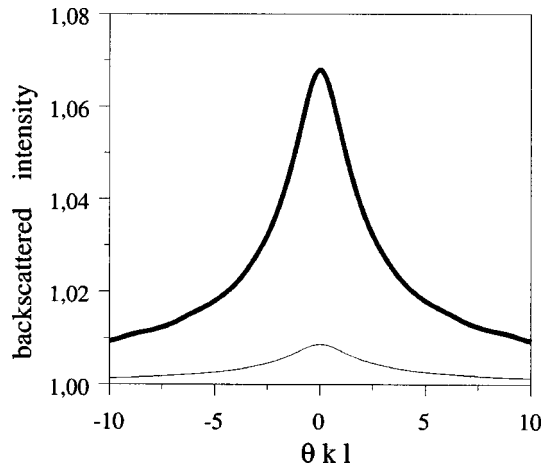


Fig. 5. Role of Raman transitions in CBS enhancement. We plot the CBS peaks obtained in the $h||h$ channel with a MC simulation for a uniform, spherical cloud of optical thickness $b = 10$ ($F = 3 \rightarrow F' = 4$ of Rb^{85}). The bold curve corresponds to both Rayleigh and Raman transitions contributing to the interference. The light curve is obtained by assuming no contribution of the Raman processes to the CBS interference and is clearly not consistent with the data in Fig. 2.

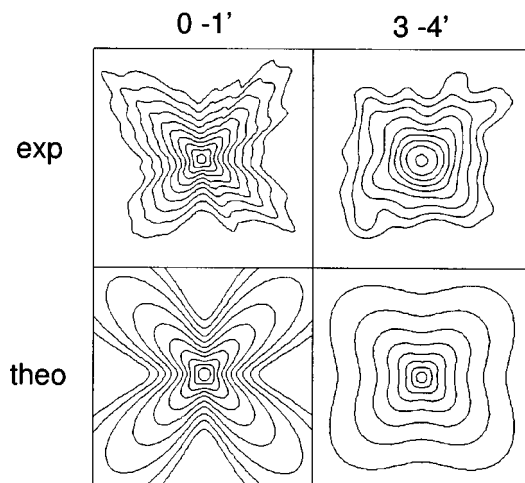


Fig. 6. Anisotropies of the CBS pattern for atomic scatterers in the $lin \perp lin$ channel. First row, experiment; second row, theory. First column, $F = 0 \rightarrow F' = 1$ transition of Sr^{88} (dipole pattern); second column, $F = 3 \rightarrow F' = 4$ transition of Rb^{85} . The CBS peak for Rb^{85} (right column) is cushion-shaped instead of cloverleaf-shaped as for Sr^{88} (left column).

pole scatterers. A variety of CBS shapes can thus be observed depending on the type of scatterer and on the polarization channel.²²

An example is shown in Fig. 6, where we compare the CBS shape in the $lin \perp lin$ channel for Sr^{88} (left column: top, experiment; bottom, theory) and Rb^{85} (right column). For dipole scatterers (or a $F = 0 \rightarrow F' = 1$ transition), the CBS peak in the $lin \perp lin$ channel has a distinctive cloverleaf shape. The theoretical prediction assumes double scattering only and clearly shows the difference between a $F = 0 \rightarrow F' = 1$ and a $F = 3 \rightarrow F' = 4$ transition.¹² In the case of Rb^{85} ($F = 3 \rightarrow F' = 4$), the same overall symmetries are observed since the purely statistical average over all Zeeman sublevels introduces no new anisotropies, but the anisotropic features are strongly rounded.

5. CONCLUSION

In this paper we have shown theoretical and experimental results for coherent backscattering of light by atomic scatterers, analyzing in detail the impact of the quantum internal structure of the atoms on the enhancement factor. For all transitions studied in the experiment [Rb^{85} ($F = 3 \rightarrow F' = 4$), Rb^{85} ($F = 2 \rightarrow F' = 1$), Rb^{87} ($F = 2 \rightarrow F' = 3$), and Sr^{88} ($F = 0 \rightarrow F' = 1$)], we found excellent agreement between theory and experiment, thus confirming that any internal structure different from an $F = 0 \rightarrow F' = 1$ transition yields strongly reduced CBS cones. The Zeeman degeneracy has an important impact on the interference contrast in CBS experiments. As we have shown, the enhancement factor is reduced even in the helicity-preserving channel as the result of a single-scattering contribution from degenerate Raman processes and a reduced ratio between the maximally crossed terms and the ladder term. The precise enhancement factor depends on the distribution among scattering orders and hence on the optical thickness, as well as on the geometry of the sample and the illumination.

As CBS is often associated with weak localization, it would be interesting to connect the measured quantities and identify common physical phenomena. One could then try to evaluate the impact of the quantum internal structure of the scatterers, clarified for CBS, on weak and perhaps on strong localization. We predict that when quasi-resonant excitation is used, the internal structure of the scatterer will have a very important effect and might possibly make the observation of strong localization of light waves by atoms with a degenerate ground state (such as Rb^{87} or Rb^{85}) more difficult, if not impossible. This has been our main motivation in setting up an experiment with Sr^{88} atoms where, even for resonant excitation, a $L = 0$ to $L' = 1$ transition seems to be an excellent model as proven by the experiments reported here.

ACKNOWLEDGMENTS

Financial support from Centre National de la Recherche Scientifique and the Provence Alpes Côte d'Azur Region is acknowledged. The Laboratoire Kastler Brossel de

l'Université Pierre et Marie Curie et de l'École Normale Supérieure is UMR 8552 du CNRS. CPU time on various computers was provided by Institut du Développement et des Ressources en Informatique Scientifique.

Corresponding author D. Wilkowski may be reached by e-mail to David.Wilkowski@inln.cnrs.fr.

*Present address, Stanford University, Stanford, California 94305-4060.

**Present address, Centre de Physique Théorique, Campus de Luminy, Case 907, 13288 Marseille Cedex 9, France.

***Present address, University of Southampton, Southampton S017 1BJ, UK.

REFERENCES

1. "Mesoscopic quantum physics," *Les Houches Summer School Proceedings, Vol. LXI*, E. Akkermans, G. Montambaux, J.-L. Pichard, and J. Zinn-Justin, eds. (North-Holland, Amsterdam, 1996).
2. S. John, "Strong localization of photons in certain disordered dielectric superlattices," *Phys. Rev. Lett.* **58**, 2486–2489 (1987).
3. E. Yablonovitch, "Inhibited spontaneous emission in solid-state physics and electronics," *Phys. Rev. Lett.* **58**, 2059–2062 (1987).
4. *Photonic Crystals and Light Localization in the 21st Century*, C. M. Soukoulis, ed. (Kluwer, Dordrecht, The Netherlands, 2001).
5. "Diffuse waves in complex media," *NATO Science Series: C, Mathematical and Physical Sciences, Vol. 531*, J. P. Fouque, ed. (Kluwer, Dordrecht, The Netherlands, 1999).
6. D. S. Wiersma, P. Bartolini, A. Lagendijk, and R. Righini, "Localization of light in a disordered medium," *Nature* **390**, 671–673 (1997).
7. F. Scheffold, R. Lenke, R. Tweer, and G. Maret, "Localization or classical diffusion of light?" *Nature* **398**, 206–207 (1999).
8. J. Gómez Rivas, R. Sprik, A. Lagendijk, L. D. Noordam, and C. W. Rella, "Static and dynamic transport of light close to the Anderson localization transition," *Phys. Rev. E* **63**, 046613 (2001).
9. G. Labeyrie, F. de Tomasi, J.-C. Bernard, C. A. Müller, Ch. Miniatura, and R. Kaiser, "Coherent backscattering of light by cold atoms," *Phys. Rev. Lett.* **83**, 5266–5269 (1999).
10. G. Labeyrie, C. A. Müller, D. S. Wiersma, Ch. Miniatura, and R. Kaiser, "Observation of coherent backscattering of light by cold atoms," *J. Opt. B: Quantum Semiclassical Opt.* **2**, 672–685 (2000).
11. Y. Bidet, B. Klappauf, J. C. Bernard, D. Delande, G. Labeyrie, C. Miniatura, D. Wilkowski, and R. Kaiser, "Coherent light transport in a cold strontium cloud," *Phys. Rev. Lett.* **88**, 203902 (2002).
12. G. Labeyrie, Ch. Miniatura, C. A. Müller, O. Sigwarth, D. Delande, and R. Kaiser, "Hanle effect in coherent backscattering," *Phys. Rev. Lett.* **89**, 163901 (2002).
13. G. Labeyrie, D. Delande, C. A. Müller, Ch. Miniatura, and R. Kaiser, "Coherent backscattering of light by an inhomogeneous cloud of cold atoms," *Phys. Rev. A* **67**, 033814 (2003).
14. P. Kulatunga, C. I. Sukenik, S. Balik, M. D. Havey, D. V. Kupriyanov, and I. M. Sokolov, "Measurement of correlated multiple light scattering in ultracold atomic ^{85}Rb ," *Phys. Rev. A* **68**, 033816 (2003).
15. T. Jonckheere, C. A. Müller, R. Kaiser, Ch. Miniatura, and D. Delande, "Multiple scattering of light by atoms in the weak localization regime," *Phys. Rev. Lett.* **85**, 4269–4272 (2000).
16. C. A. Müller, T. Jonckheere, C. Miniatura, and D. Delande, "Weak localization of light by cold atoms: The impact of quantum internal structure," *Phys. Rev. A* **64**, 053804 (2001).
17. C. A. Müller and Ch. Miniatura, "Multiple scattering of light by atoms with internal degeneracy," *J. Phys. A* **35**, 10163–10188 (2002).
18. D. V. Kupriyanov, I. M. Sokolov, P. Kulatunga, C. I. Sukenik, and M. D. Havey, "Coherent backscattering of light in atomic systems: Application to weak localization in an ensemble of cold alkali metal atoms," *Phys. Rev. A* **67**, 013814 (2003).
19. G. Labeyrie, D. Delande, C. A. Müller, Ch. Miniatura, and R. Kaiser, "Coherent backscattering of light by cold atoms: theory meets experiment," *Europhys. Lett.* **61**, 327–333 (2003).
20. A. Lagendijk and B. A. van Tiggelen, "Resonant multiple scattering of light," *Phys. Rep.* **270**, 143–215 (1996).
21. M. C. W. van Rossum and Th. M. Nieuwenhuizen, "Multiple scattering of classical waves: microscopy, mesoscopy, and diffusion," *Rev. Mod. Phys.* **71**, 313–371 (1999).
22. M. J. Rakovic, G. W. Kattawar, M. Mehrbeolu, B. D. Cameron, L. V. Wang, S. Rastegar, and G. L. Cote, "Light backscattering polarization patterns from turbid media: theory and experiment," *Appl. Opt.* **38**, 3399 (1999).